

Destabilization of a laminar flow in a rectangular channel by transversely-oriented wall corrugation

J. SZUMBARSKI¹⁾, S. BŁOŃSKI²⁾

¹⁾*Institute of Aeronautics and Applied Mechanics
Warsaw University of Technology
Nowowiejska 24
00-665 Warszawa, Poland
e-mail: jasz@meil.pw.edu.pl*

²⁾*Institute of Fundamental Technological Research
Polish Academy of Science
Pawińskiego 5B
02-106 Warszawa, Poland
e-mail: sblonski@ippt.gov.pl*

LINEAR STABILITY OF THE FLOW through the transversely corrugated channel with flat sidewalls is investigated numerically. Two variants of the wall corrugation are considered: symmetric sinusoidal waviness of the top and bottom walls and one-sided corrugation, i.e., one of the walls remains flat. Spectrally accurate Galerkin method formulated in a transformed domain is used for the solution of the main flow and linear stability equations. Unstable normal modes have been identified and their parametric variation has been determined. The results show that for sufficiently large aspect ratios, the influence of the sidewalls is weak and the stability properties resemble those of the spanwise-periodic channel (investigated recently by the first author). It means that an appropriately designed transversal corrugation may be regarded as a promising method for passive enhancement of mixing in laminar regime.

Key words: hydrodynamic stability, wavy channel, wall corrugation, laminar mixing.

Copyright © 2011 by IPPT PAN

Notations

x, y, z	spatial variables in the physical domain,
ξ, η	spatial variables in the computational domain,
L	dimensionless half-width of the channel (also, the aspect ratio of the channel section),
Re	the Reynolds number,
$W_{\text{ref}}, Q_{\text{ref}}$	velocity and volumetric flow rate of the flow in the rectangular channel,
$h(x)$	function describing the form of the wall corrugation,
W_m	velocity profile of the main (undisturbed) flow,
\mathbf{V}_m, P_m	main flow velocity and pressure fields,

u, v, w	components of the velocity field of the flow disturbances,
p	pressure field of the flow disturbances,
$\hat{u}, \hat{v}, \hat{w}$	Fourier amplitudes of the velocity components of the normal mode,
\hat{p}	Fourier amplitude of the pressure field of the normal mode,
β	streamwise wave number of the normal mode,
$\sigma = \sigma_R + \sigma_I i$	complex frequency of the normal mode,
T_k	Chebyshev polynomial of the k -th order,
$\{b_I^V, I = 1, \dots, N\}$	the ensemble of the orthogonal basic functions used for the approximation of Fourier amplitudes $\hat{u}, \hat{v}, \hat{w}$.

1. Introduction

THE ENHANCEMENT OF TRANSPORT CAPABILITIES of internal laminar flows is of fundamental importance in numerous applications in heat transfer, biotechnology and microfluidics. These capabilities can be acquired only through intense mixing which, in turn, necessitates existence of sufficiently complex, three-dimensional and preferably time-dependent vortex structures. Such form of the velocity field in the otherwise simple and usually unidirectional flow can be brought about by various methods including geometric modifications (wall waviness, application of surface-mounted obstacles or vortex generators), external forcing (pulsations or the pressure gradient, mounting of vibrating elements, using wall transpiration, etc.) or the combination of both.

During the last four decades, different variants of such solutions have been proposed and analyzed, both numerically and experimentally. GOLDSTEIN and SPARROW [1] investigated the kinematic structures and mass transfer through the divergent-convergent channel with symmetrically corrugated arc-shaped walls. This research was motivated mostly by the need for improvement of mixing efficiency in the flows through oxygenators. Later, numerical investigations of two-dimensional flow in a divergent-convergent symmetric channel with sinusoidal walls were performed by SOBEY [2] and verified experimentally by STEPHANOFF *et al.* [3]. Systematic investigations of flows through channels with sinusoidal walls have been carried out since the middle 80s in Japan, mostly by Nishimura and his co-workers. Different variant have been considered including stationary flows [4] as well as flows driven by oscillatory [5, 6] or pulsatile pressure gradient [7, 8].

From the practical point of view, it is particularly interesting to consider flows, which acquire complex structure through natural instability rather than by external forcing. It has been demonstrated in a number of works [9–11] that significant improvement of heat/mass transport in laminar regime may be obtained only if boundaries of a flow domain are shaped properly to induce low-Reynolds number instability and the excited normal modes are oscillatory, i.e., they have a form of travelling waves. In a divergent-convergent channel with

sinusoidal and streamwise-oriented wall waviness, the oscillatory unstable mode has been found for the Reynolds number exceeding 200 and more than three-fold heat transfer enhancement has been demonstrated. Unfortunately, such spectacular effect appears usually at the price of an excessive hydraulic resistance, which can be even several times larger than in the reference “smooth” flow.

The possibility of the low-Reynolds number destabilization of the channel flows has been studied during last two decades by a number of authors. Majority of this research focuses of the wall waviness which is two-dimensional and streamwise-oriented, i.e., the lines of constant elevation of the wall are perpendicular to the main flow direction. Such type of the wall corrugation is referred in this paper to as the longitudinal one, see Fig. 1a. In particular, it has been shown in [12] that, using a longitudinal wall corrugation with an appropriate wavelength and sufficiently large amplitude, the critical Reynolds number Re_L can be reduced to the values as low as 100. The unstable normal mode is oscillatory, i.e., the disturbance has the form of a travelling wave meaning that

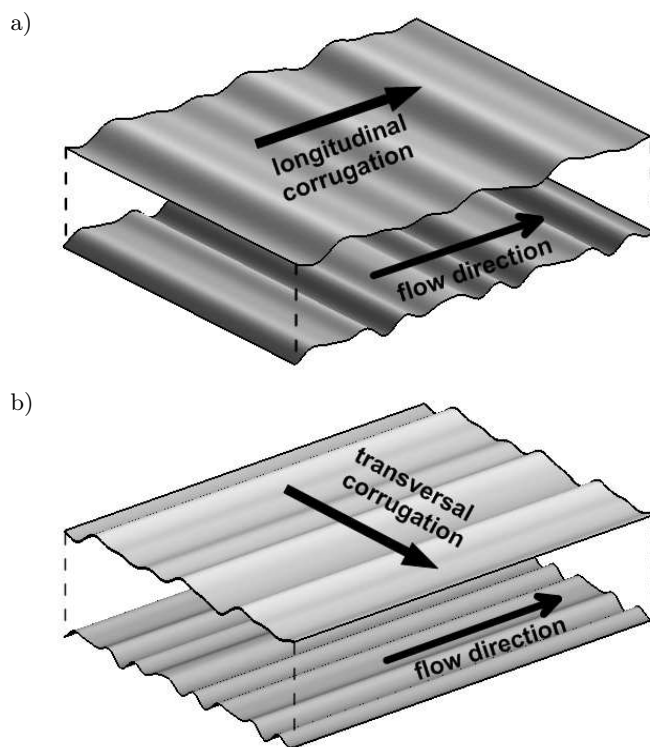


FIG. 1. Different orientations of wall corrugation with respect to the flow direction:
a) longitudinal, b) transversal.

the disturbed flow is expected to be time-dependent. Other unstable mode, having the form of the stationary wave, has been also identified. The stationary disturbances are three-dimensional and, for lower corrugation amplitudes, their critical Reynolds number is smaller than for the oscillatory mode. The effect of instability of the travelling wave disturbances on the effectiveness of heat transfer in the flow through a divergent-convergent channel was investigated numerically by BLANCHER *et al.* in [13]. Recently, the same authors have carried out numerical analysis of spatially developing nonlinear instabilities in such a flow [14]. In other papers [15–17], the longitudinally oriented wall waviness has been considered as the simplified model of unidirectional wall roughness. Consequently, the amplitudes taken into account are rather small, yet some aspects of the analysis, especially in the numerical approach (application of immersed boundaries and domain transformation) are of some relevance also to the current study.

Surprisingly enough, the number of works devoted to the stability of laminar flows in transversely corrugated channels (see Fig. 1b) is rather limited. Such type of geometrical modifications attracted some attention since late 80's due to their relation to the surface elements called the riblets. The main objective of this research was to explore the potential offered by the riblets in terms of reduction of the skin-friction in the turbulent boundary layer (see [18] for the comprehensive review). A few papers on the influence of the riblets on the laminar-turbulent transition in the boundary layers have been also published in mid 90's, see the brief account of the main results in the seventh section of the monograph [19]. In the context of the current study, the most important reference is [20], where the numerical analysis of the channel flow instability induced by a short-wave and high-amplitude, transversely oriented wall corrugation (mimicking the presence of riblets) has been presented. It has been shown that the critical Reynolds number of the most unstable normal mode can drop under the value of 2600 (compared to $Re_L = 5772$ of the smooth configuration, i.e., plain Poiseuille flow).

The result obtained in [20] might suggest that the application of the transverse wall corrugation is not a right way to obtain flow destabilization at really low Reynolds numbers. However, one has to keep in mind that the aim of the analysis in [20] was to assess influence of the ribbed surface on the stability of a particular class of disturbances (the Orr-Sommerfeld modes) rather than looking for opportunities of mixing enhancement. Thus, the true lesson learnt from [20] is that the Orr-Sommerfeld modes are not the candidates for flow destabilization at low Reynolds numbers and, perhaps, also the considered geometry of the corrugation is probably not proper for this purpose.

The problem of low-Reynolds-number destabilization of the Poiseuille flow by means of transversely-oriented wall waviness has been taken up by the author

of the current study, and the most important findings were published in his habilitation thesis [21] in 2007. Early calculations showed that Orr-Sommerfeld modes respond rather weakly to the transverse wall waviness. This conclusion is consistent with the findings of the earlier study [20]. However, further analysis has revealed existence of a Squire mode which is particularly sensitive to the transverse corrugation with rather large wavelength (3–5 times larger than the average height of the channel’s section). Destabilization of this (otherwise stable) mode is particularly strong when the corrugation is applied simultaneously to both channel’s walls, with equal amplitudes and the opposite phase. On the other hand, double-sided corrugation with zero phase-shift does not seem to have any effect on flow stability at low and moderate Reynolds numbers. The explanation of this fact can be formulated in terms of spanwise modulation of the main flow velocity. The magnitude of this modulation is the function of the phase shift between bottom and top wall’s corrugation. Sufficiently large amplitude of the spanwise modulation (accompanied by appearance of inflection points in the velocity profile) is necessary for flow destabilization. The maximal amplitude of the modulation is attained when the wall corrugations are exactly in the opposite phase. If the phase shift is zero, the situation is quite different: the modulation basically disappears and the flow destabilization is absent.

It has been shown in the work [21] that the application of the opposite-phase double-sided sinusoidal wall waviness with properly chosen wavelength and the amplitude equal 10% of the average channel height, is able to reduce the critical Reynolds number Re_L to the value of 215. In continuation of this investigation (see [22]), larger corrugation amplitudes have been considered and further reduction to the spectacular value of $Re_L = 58$ has been achieved at the corrugation amplitude equal to about 20% of the average channel height. Since any further attempts to increase the amplitude of the corrugation resulted in some increase of Re_L , thus one can safely assume that the value of 58 is very close to the lowest value possible.

Another interesting finding of the investigations presented in [21] and [22] is that the low-Reynolds-number flow destabilization is not accompanied by any significant increase of the hydraulic resistance. Indeed, the value of the wavelength of the most destabilizing transversal corrugation happens to coincide almost exactly with the value of the wavelength for which the flow resistance remains nearly unchanged, i.e. it is the same as for the “smooth” Poiseuille flow. Another important property is that the critical Reynolds number Re_L depends mostly on the spectral (Fourier) structure of the corrugation shape. More specifically, if two different shapes of the wall corrugation share the same Fourier mode with a wavenumber from an appropriate range, then the corresponding values of Re_L will be very close irrespectively to other details of these shapes. It means in particular, that the actual “depth” of the corrugation is irrelevant

– the flow may remain stable in the presence of even large corrugation if the Fourier spectrum of the wall shape does not contain a “dangerous” wavenumber.

Yet another result of the research reported in [21] and [22] was the determination of the spatial structure of the unstable Squire mode. The velocity field of this mode assumes the form of a vortex array, which is periodic in both streamwise and spanwise directions. Since the real part of the corresponding complex frequency is nonzero, this pattern moves downstream as the travelling disturbance wave. Therefore one can expect that the flow resulting from a nonlinear saturation process of small disturbances will exhibit oscillations which should significantly improve its mixing capabilities. This expectation has been positively verified by the direct numerical simulations using FLUENT [23].

In aim of the current research is to investigate numerically linear stability of the laminar flow in the channel of finite width, which is one step towards more realistic configurations than those considered in earlier works [21] and [22]. More specifically, we assume that the bottom and top walls of the channel are arbitrarily corrugated while the sidewalls are flat and parallel.

The analysis is of the temporal type and consists in determination of the least stable (or most unstable) eigensolutions (normal modes) of the linear stability equations. Once such modes are indentified, their variation with respect to the geometric characteristics of the wall corrugation, the streamwise wavenumber, and the Reynolds number is investigated. The ultimate goal of the analysis is to assess the role of the channel sidewalls in the effect of low-Reynolds-number instability. This time, the reference case is the flow through the channel with rectangular section of the same aspect ratio. It is well known (see [24]) that the critical Reynolds number Re_L of the rectangular channel of a finite span is always larger than its value for the plane Poiseuille flow. By analogy, a certain increase of Re_L is expected when the wall waviness is implemented for the channel with sidewall rather than for the periodic channel of infinite width. The key issue is: assuming that the aspect ratio of the channel section is large (but not too large), is the value of Re_L still small enough to make the transversely-oriented wall corrugation a worth considering option?

This paper provides an extended account of the theory and numerical results reported recently on the European Fluid Mechanics Conference EFMC-8 [25]. The contents of the paper can be summarized as follows. In the Sec. 2, the mathematical formulation for the main (undisturbed) flow and for the evolution of small disturbances has been provided. In the Sec. 3, the numerical approach to the main flow and to the linear stability equations has been described. The results of the parametric study of the unstable modes are presented in the Sec. 4. Finally, the summary, conclusion and perspectives of further investigations are presented shortly in the Sec. 5.

2. Mathematical formulation

2.1. Flow in the rectangular channel

Consider first the flow in the rectangular channel, depicted in Fig. 2, which will serve in this study as the reference case. The vertical distance between bottom and top walls will be referred to as the channel height, while the distance between the sidewalls is called the channel width or span. The dimensionless coordinates are used such that the channel height is equal to 2 and the channel width is equal to $2L$. The ratio between the channel width and the channel height, equal to L , will be called the channel aspect ratio.

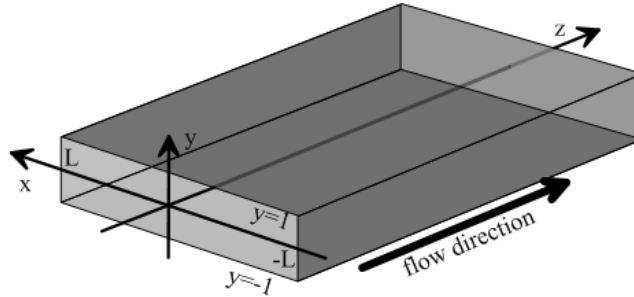


FIG. 2. Channel with rectangular cross-section.

In the coordinate system chosen as shown in Fig. 2, the only nonzero component of the velocity field is the z -component given by the following non-dimensional formula:

$$(2.1) \quad W_{\text{ref}}(x, y) = 1 - y^2 + 4 \sum_{k=1}^{\infty} \frac{(-1)^k \cosh(\alpha_k x)}{\alpha_k^3 \cosh(\alpha_k L)} \cos(\alpha_k y), \quad \alpha_k = \frac{2k-1}{2}\pi.$$

The function W_{ref} is the solution to the following boundary value problem

$$(2.2) \quad \Delta W_{\text{ref}} \equiv \frac{\partial^2 W_{\text{ref}}}{\partial x^2} + \frac{\partial^2 W_{\text{ref}}}{\partial y^2} = -2, \quad (x, y) \in \Omega,$$

$$W_{\text{ref}}|_{\partial\Omega} = 0,$$

where $\Omega = \{(x, y) : -L \leq x \leq L, -1 \leq y \leq 1\}$. In this study, the flow defined by (2.1) is considered as a modification of the associated non-dimensional Poiseuille flow

$$(2.3) \quad W_P(x, y) = 1 - y^2.$$

The modification is caused by the presence of the side walls at $x = -L$ and $x = L$. Both the (2.1) and (2.3) flows are driven by the same non-dimensional

pressure gradient; its dimensionless value is

$$(2.4) \quad G_p = -\frac{2}{\text{Re}}.$$

In the formula (2.4), the symbol Re denotes the Reynolds number defined as follows:

$$(2.5) \quad \text{Re} = \frac{w_P^{\max} H}{\nu},$$

where ν denotes the kinematic viscosity of a fluid and w_P^{\max} denotes the maximal value of the velocity of the Poiseuille flow between parallel walls separated by the distance of $2H$.

The non-dimensional volumetric flow rate corresponding to the velocity distribution (2.1) can be computed from the following formula:

$$(2.6) \quad \begin{aligned} Q_{\text{ref}} = Q_{\text{ref}}(L) &= \frac{8}{3}L \left[1 - \frac{6}{L} \sum_{k=1}^{\infty} \frac{\tanh(\alpha_k L)}{\alpha_k^5} \right] \\ &= Q_P \left[1 - \frac{6}{L} \sum_{k=1}^{\infty} \frac{\tanh(\alpha_k L)}{\alpha_k^5} \right]. \end{aligned}$$

In the above, the symbol $Q_P = 8L/3$ denotes the non-dimensional flow rate of the associated Poiseuille flow (2.3) computed for the transversal segment having the width of $2L$, i.e., the same as the rectangular channel. Clearly, $Q_{\text{ref}} < Q_P$ because the fluid velocity near the sidewalls of the rectangular channel decreases to zero. The infinite series term in the formula (2.6) can be interpreted as the measure of increase in the flow resistance caused by the sidewalls.

2.2. Main flow

Consider now the flow in the channel with transversely corrugated walls. Two types of wall corrugation are considered in this study:

1. Channel with symmetric corrugation of the bottom and top walls (see Fig. 3a), i.e., described by the dimensionless formula

$$(2.7) \quad y_t(x) \equiv h(x) = -y_b(x).$$

2. Channel with one-sided corrugation (see Fig. 3b), i.e., with the flat bottom wall and wavy top wall (considered as the model of the experimental setup in [23])

$$(2.8) \quad y_t(x) \equiv h(x), \quad y_b(x) \equiv 0.$$

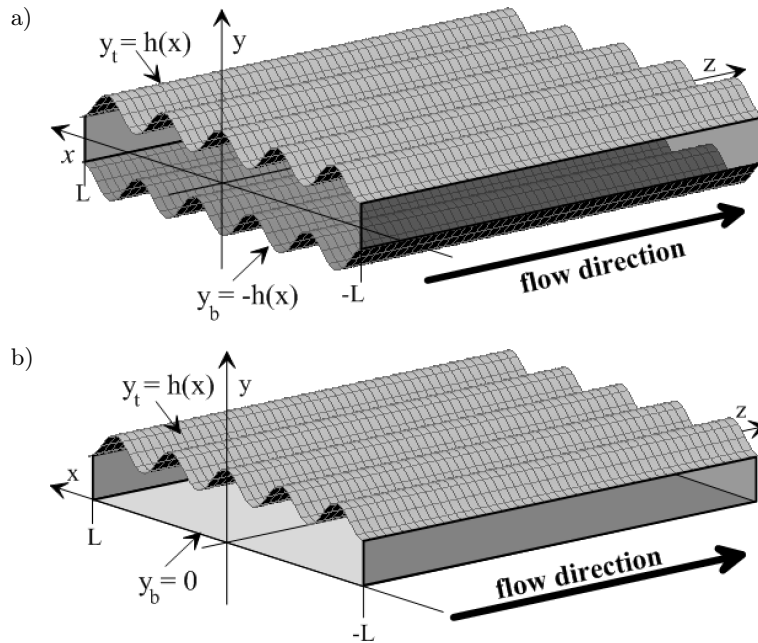


FIG. 3. Different variants of transversal wall corrugation: a) symmetric corrugation, b) one-sided corrugation.

In both cases, the sidewalls are flat and the range of the x coordinate is $-L \leq x \leq L$, i.e., the width of the channel remains equal to $2L$. It is assumed that the average value of the function $h = h(x)$ is 1 in the symmetric corrugation case or it is equal to 2 in the case of one-sided corrugation. Thus, irrespectively of the corrugation variant, the average height of the channel is equal to 2 and the area of the channel section is equal to $4L$. The aspect ratio of the channel section, which is defined as the ratio between the channel width and average height, is equal to L .

The flow in the wavy channel is driven by the same steady pressure gradient as the reference flow (2.1) in the rectangular channel. This flow is also unidirectional, i.e., the only nonzero component of the velocity field is the z -component $W_m = W_m(x, y)$. The function W_m is the solution to the following boundary value problem analogous to (2.2), namely

$$(2.9) \quad \Delta W_m \equiv \frac{\partial^2 W_m}{\partial x^2} + \frac{\partial^2 W_m}{\partial y^2} = -2, \quad (x, y) \in \Omega,$$

$$W_m|_{\partial\Omega} = 0,$$

where this time the symbol Ω denotes the channel section (in the plane $z = \text{const}$) and $\partial\Omega$ denotes the contour of Ω .

2.3. Linear stability analysis

The stability analysis begins with the derivation of the equations which govern the dynamics of small disturbances imposed on the main flow. The disturbed velocity and pressure fields can be written as a sum of the main flow and the time-dependent and three-dimensional disturbances

$$(2.10) \quad \begin{aligned} \mathbf{V}(t, x, y, z) &= \mathbf{V}_m(x, y) + \mathbf{v}(t, x, y, z) \\ &= [0, 0, W_m(x, y)] + [u, v, w](t, x, y, z), \\ P(t, x, y, z) &= P_m(z) + p(t, x, y, z). \end{aligned}$$

Next, the formulas (2.10) are plugged into the Navier-Stokes and continuity equations. Since the disturbances are assumed to be small, the nonlinear terms are removed and the following set of linear differential equations is obtained:

$$(2.11) \quad \begin{aligned} \partial_t u + W_m \partial_z u &= -\partial_x p + \frac{1}{\text{Re}}(\partial_{xx} + \partial_{yy} + \partial_{zz})u, \\ \partial_t v + W_m \partial_z v &= -\partial_y p + \frac{1}{\text{Re}}(\partial_{xx} + \partial_{yy} + \partial_{zz})v, \\ \partial_t w + W_m \partial_z w + u \partial_x W_m + v \partial_y W_m &= -\partial_z p + \frac{1}{\text{Re}}(\partial_{xx} + \partial_{yy} + \partial_{zz})w, \\ \partial_x u + \partial_y v + \partial_z w &= 0. \end{aligned}$$

The velocity field (2.10) vanishes at $\partial\Omega$, which implies the following boundary conditions for the velocity field disturbances

$$(2.12) \quad [u, v, w]|_{\partial\Omega} = 0.$$

In general, the initial conditions must be also formulated

$$(2.13) \quad [u, v, w]|_{t=0} = [u_0, v_0, w_0].$$

Since the velocity W_m of the basic flow does not depend on variable z , the Eqs. (2.11) admit particular solutions (normal modes) in the following form:

$$(2.14) \quad [u, v, w, p](t, x, y, z) = [\hat{u}, \hat{v}, \hat{w}, \hat{p}](x, y) \exp[i(\beta z - \sigma t)] + c.c.$$

In the above, the hat symbols refer to the complex amplitude functions and the symbol ‘‘c.c.’’ stands for the complex conjugate terms. The quantity $\sigma = \sigma_R + i\sigma_I$ is the complex frequency of the normal mode. The symbol β denotes the spanwise wave number of the flow disturbance, which is assumed to be z -periodic with the period equal $2\pi/\beta$. This assumption concerns also the pressure disturbances, which implies that the average value of the streamwise pressure gradient of the

disturbed flow remains equal to the pressure gradient of the main (undisturbed) flow.

After insertion of the normal mode formula (2.14) to the Eqs. (2.11), one obtains

$$\begin{aligned}
 (2.15) \quad & -i\sigma\hat{u} + i\beta W_m \hat{u} = -\partial_x \hat{p} + \frac{1}{\text{Re}}(\Delta - \beta^2)\hat{u}, \\
 & -i\sigma\hat{v} + i\beta W_m \hat{v} = -\partial_y \hat{p} + \frac{1}{\text{Re}}(\Delta - \beta^2)\hat{v}, \\
 & -i\sigma\hat{w} + i\beta W_m \hat{w} + \hat{u}\partial_x W_m + \hat{v}\partial_y W_m = -i\beta\hat{p} + \frac{1}{\text{Re}}(\Delta - \beta^2)\hat{w}, \\
 & \partial_x \hat{u} + \partial_y \hat{v} + i\beta\hat{w} = 0.
 \end{aligned}$$

From (2.12) one concludes that the amplitude functions of the velocity components should satisfy the homogeneous boundary condition at the channel section contour

$$(2.16) \quad [\hat{u}, \hat{v}, \hat{w}]|_{\partial\Omega} = 0.$$

The main goal of the linear stability analysis is to identify conditions in which at least one unstable eigensolution of the boundary value problem (2.15)–(2.16) exists. The normal mode is unstable if and only if the imaginary part σ_I of its complex frequency σ is positive. In the context of flow destabilization, it is particularly interesting to determine the critical Reynolds number Re_L , i.e., the maximal value of the Reynolds number such that all normal modes are either attenuated ($\sigma_I < 0$) or – at most – neutrally stable ($\sigma_I = 0$). It follows that for $\text{Re} > \text{Re}_{\text{crt}}$ there exists at least one normal mode which grows exponentially in time. Since the magnitude of disturbances in the linear theory is arbitrarily small, the flow with $\text{Re} > \text{Re}_{\text{crt}}$ is unconditionally unstable.

3. Numerical method

3.1. Domain transformation

In order to determine numerically the form of the main flow and analyze linear stability characteristics, the transformation of the physical domain Ω to the computational domain $[-1, 1]^2$ is applied. The particular variant of this mapping depends on the type of the corrugation:

1. Symmetric corrugation (see Fig. 4a).

In this case, the transformation from physical to computational domain is defined as follows

$$\begin{aligned}
 (3.1) \quad & \xi = x/L, \\
 & \eta = y/h(x) = y/[LH(x/L)],
 \end{aligned}$$

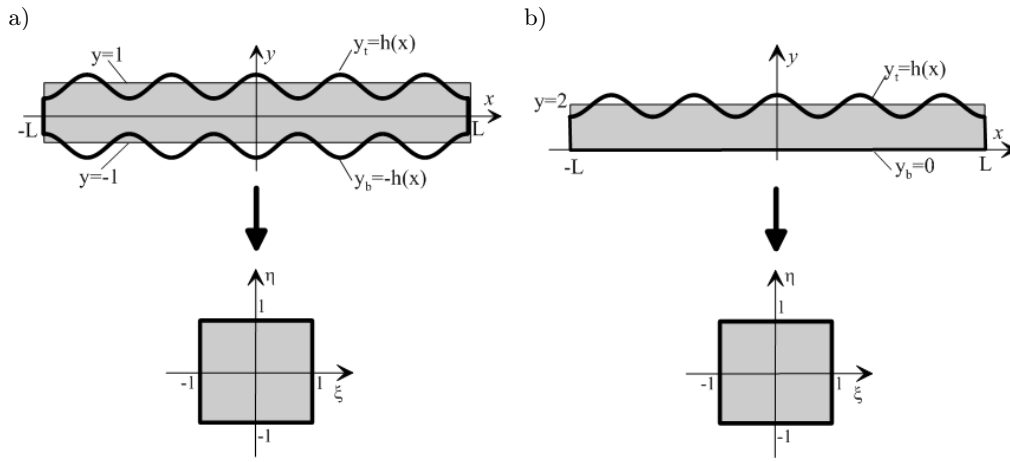


FIG. 4. Mapping from physical domain to the computational domain: a) symmetric corrugation, b) one-sided corrugation.

where

$$(3.2) \quad H(\xi) = h(L\xi)/L.$$

The corresponding inverse mapping is given by the formula

$$(3.3) \quad \begin{aligned} x &= L\xi, \\ y &= \eta h(L\xi) = L\eta H(\xi). \end{aligned}$$

2. One-sided corrugation (see Fig. 4b).

In this case, the transformation from physical to computational domain is defined as follows:

$$(3.4) \quad \begin{aligned} \xi &= x/L, \\ \eta &= 2y/h(x) - 1 = 2y/[LH(x/L)] - 1, \end{aligned}$$

where the function H is defined by (3.2). The inverse mapping is defined by the formula

$$(3.5) \quad \begin{aligned} x &= L\xi, \\ y &= \frac{1}{2}(\eta + 1)h(L\xi) = \frac{1}{2}(\eta + 1)LH(\xi). \end{aligned}$$

3.2. Numerical method for the main flow

The boundary value problem (2.2) is transformed to the following form:

$$(3.6) \quad \begin{aligned} \tilde{\Delta}W_m(\xi, \eta) &= -2, \quad (\xi, \eta) \in [-1, 1]^2, \\ W_m(\xi = \pm 1, \eta = \pm 1) &= 0, \end{aligned}$$

where the main flow velocity W_m is expressed in the variables ξ and η , and the symbol $\tilde{\Delta}$ denotes the transformed Laplace operator defined as

$$(3.7) \quad \tilde{\Delta} = L^{-2}(\partial_{\xi\xi} - 2a_{\xi\eta}\partial_{\xi\eta} + a_{\eta\eta}\partial_{\eta\eta} + a_{\eta}\partial_{\eta}).$$

The functional coefficients in the formula (3.7) can be expressed as follows

$$(3.8) \quad \begin{aligned} a_{\xi\eta} &= a(\eta)g_1(\xi), & a_{\eta\eta} &= \gamma^2g_2^2(\xi) + a^2(\eta)g_1^2(\xi), \\ a_{\eta} &= a(\eta)[2g_1^2(\xi) - g_3(\xi)], \end{aligned}$$

where

$$(3.9) \quad g_1(\xi) = H'(\xi)/H(\xi), \quad g_2(\xi) = 1/H(\xi), \quad g_3(\xi) = H''(\xi)/H(\xi),$$

$$(3.10) \quad a(\eta) = \begin{cases} \eta & \text{for symmetric corrugation,} \\ \eta + 1 & \text{for one-sided corrugation;} \end{cases}$$

$$(3.11) \quad \gamma = \begin{cases} 1 & \text{for symmetric corrugation,} \\ 2 & \text{for one-sided corrugation.} \end{cases}$$

The boundary value problem (3.6) can be solved numerically by means of the spectral method. To this aim, the following polynomial functions are defined in the computational domain $[-1, 1]^2$:

$$(3.12) \quad \begin{aligned} \phi_{i,j}(\xi, \eta) &= [T_{i+2}(\xi) - T_i(\xi)][T_{j+2}(\eta) - T_j(\eta)], \\ & \quad i = 0, \dots, N_{\xi}, \quad j = 0, \dots, N_{\eta}. \end{aligned}$$

In the above formula, the general symbol T_k refers to the standard Chebyshev polynomial of the order k . Note that the formula (3.12) implies that each function $\phi_{i,j}$ vanishes identically at the boundary of the computation domain.

In the next step, the set of the functions (3.12) is re-numerated by a single index $I = I(i, j)$. Finally, the Gram–Schmidt orthogonalization is applied to obtain the orthonormal system of the basic functions $\{b_I^V, I = 1, \dots, N\}$, where

$$N = (N_{\xi} + 1) \cdot (N_{\eta} + 1).$$

The property of orthogonality means that the following conditions hold

$$(3.13) \quad \int_{-1}^1 \int_{-1}^1 b_I^V(\xi, \eta)b_J^V(\xi, \eta)\omega(\xi, \eta) d\xi d\eta = \delta_{IJ},$$

where ω is the Chebyshev weight function

$$(3.14) \quad \omega = \omega(\xi, \eta) = \left[\sqrt{(1 - \xi^2)(1 - \eta^2)} \right]^{-1}.$$

Clearly, all basic functions $\{b_I^V, I = 1, \dots, N\}$ satisfy the homogeneous boundary condition

$$(3.15) \quad b_I^V(\pm 1, \eta) = b_I^V(\xi, \pm 1) = 0.$$

The approximate solution to the boundary value problem (3.6) is sought in the form of the expansion

$$(3.16) \quad W_m(\xi, \eta) \approx \sum_{J=0}^N w_J b_J^V(\xi, \eta),$$

where the coefficients $w_I, I = 1, \dots, N$ are to be determined. To this aim, the representation (3.16) is plugged into the transformed Poisson equation in (3.6) and the obtained residuum is orthogonalized with respect to the subspace spanned by the basic functions $\{b_I^V, I = 1, \dots, N\}$. This procedure leads to the following set of conditions:

$$(3.17) \quad \int_{-1}^1 \int_{-1}^1 (\tilde{\Delta} W_m + 2) b_I^V \omega \, d\xi d\eta = 0, \quad I = 1, \dots, N.$$

After simple algebra, the system of linear equations for unknown coefficients $\{w_I, I = 1, \dots, N\}$ is obtained

$$(3.18) \quad \sum_{J=1}^N K_{IJ} w_J = r_I, \quad I = 1, \dots, N,$$

where

$$(3.19) \quad K_{IJ} = \int_{-1}^1 \int_{-1}^1 b_I^V \tilde{\Delta} b_J^V \omega \, d\xi d\eta, \quad I, J = 1, \dots, N,$$

$$(3.20) \quad r_I = -2 \int_{-1}^1 \int_{-1}^1 b_I^V \omega \, d\xi d\eta, \quad I = 1, \dots, N.$$

The linear system (3.18) can be solved using the LU factorization. In the current work, the choice of $N_\xi = 119$ and $N_\eta = 29$ (hence, $N = 3600$) provides sufficient accuracy of the main flow evaluation.

3.3. Numerical approximation of the stability equations

In order to find the form of the normal modes and associated complex frequencies, the differential eigenvalue problem (2.15)–(2.16) has to be approximated by an algebraic eigenvalue problem. As the first step of the solution procedure, the transformation of spatial coordinates is applied in the form depending on the corrugation type: (3.1)–(3.3) for symmetric corrugation, or (3.4)–(3.5) for the one-sided corrugation.

In effect, the following equations are obtained:

$$\begin{aligned}
 (3.21) \quad & -i\sigma\hat{u} + i\beta W_m\hat{u} = -\frac{1}{L}[\partial_\xi - a(\eta)g_1(\xi)\partial_\eta]\hat{p} + \frac{1}{\text{Re}}(\tilde{\Delta} - \beta^2)\hat{u}, \\
 & -i\sigma\hat{v} + i\beta W_m\hat{v} = -\frac{1}{L}\gamma g_2(\xi)\partial_\eta\hat{p} + \frac{1}{\text{Re}}(\tilde{\Delta} - \beta^2)\hat{v}, \\
 & -i\sigma\hat{w} + i\beta W_m\hat{w} + \frac{1}{L}\hat{u}[\partial_\xi - a(\eta)g_1(\xi)\partial_\eta]W_m + \frac{1}{L}\gamma\hat{v}g_2(\xi)\partial_\eta W_m \\
 & \qquad \qquad \qquad = -i\beta\hat{p} + \frac{1}{\text{Re}}(\tilde{\Delta} - \beta^2)\hat{w}, \\
 & \frac{1}{L}[\partial_\xi - a(\eta)g_1(\xi)\partial_\eta]\hat{u} + \frac{1}{L}\gamma g_2(\xi)\partial_\eta\hat{v} + i\beta\hat{w} = 0,
 \end{aligned}$$

where the function $a = a(\eta)$ and the constant γ are defined by (3.10) and (3.11). The boundary conditions accompanying the Eqs. (3.21) are

$$(3.22) \quad [\hat{u}, \hat{v}, \hat{w}](\xi = \pm 1, \eta = \pm 1) = 0.$$

The numerical approach to the system (3.21)–(3.22) is to apply the spectral discretization and the Galerkin projection method. To this aim, two sets of the basic functions – one for the velocity components and the other for the pressure field – are defined in the transformed domain $[-1, 1]^2$. The basic functions used for the velocity components are the functions $\{b_I^V, I = 1, \dots, N\}$ defined for the main flow calculations in the Sec. 3.1. The amplitude functions of the velocity components are approximated in the computational domain by the following finite expansions:

$$\begin{aligned}
 (3.23) \quad & \hat{u}(\xi, \eta) = \sum_{I=1}^N (\mathbf{u}_1)_I b_I^V(\xi, \eta), \\
 & \hat{v}(\xi, \eta) = \sum_{I=1}^N (\mathbf{u}_2)_I b_I^V(\xi, \eta), \\
 & \hat{w}(\xi, \eta) = \sum_{I=1}^N (\mathbf{u}_3)_I b_I^V(\xi, \eta),
 \end{aligned}$$

where the coefficients $(\mathbf{u}_1)_I$, $(\mathbf{u}_2)_I$, $(\mathbf{u}_3)_I$, $I = 1, \dots, N$ have to be determined.

The basic functions for the pressure disturbance field are the following polynomials of the transformed spatial coordinates:

$$(3.24) \quad b_I^p(\xi, \eta) = T_{i(I)}(\xi) T_{j(I)}(\eta), \quad I = 1, \dots, N.$$

In the above formula, the mapping $(i, j) \rightarrow I(i, j)$ from a double-index numeration to a single-index numeration has been applied. It is assumed that the total number of pressure basic functions is equal to the number of the velocity basic functions. Note also that the pressure basic functions do not vanish at the boundary of the computational domain $[-1, 1]^2$.

The pressure amplitude function \hat{p} (transformed to the computational domain) is sought in the form of the finite expansion

$$(3.25) \quad \hat{p}(\xi, \eta) = \sum_{J=1}^N (\mathbf{p})_J b_J^P(\xi, \eta),$$

where the coefficients $(\mathbf{p})_J$, $J = 1, \dots, N$ should be determined.

The discretization procedure is continued as follows. First, the expansions (3.23) and (3.25) are plugged into the transformed stability equations (3.21). Next, the residua of these equations are projected orthogonally on the appropriate functions spaces. More specifically, the residua of the first three equations are assumed to be orthogonal (in the sense of the Chebyshev inner product) to the function space spanned by the velocity basic functions, while the residuum of the last (continuity) equations is orthogonalized with respect to the subspace spanned by all pressure basic functions. The result of this procedure is the following algebraic eigenvalue/eigenvector problem:

$$(3.26) \quad \begin{aligned} -i\sigma \mathbf{u}_1 + \mathbf{C} \mathbf{u}_1 + \mathbf{D}_1 \mathbf{p} &= \mathbf{0}, \\ -i\sigma \mathbf{u}_2 + \mathbf{C} \mathbf{u}_2 + \mathbf{D}_2 \mathbf{p} &= \mathbf{0}, \\ -i\sigma \mathbf{u}_3 + \mathbf{C} \mathbf{u}_3 + \mathbf{B}_1 \mathbf{u}_1 + \mathbf{B}_2 \mathbf{u}_2 + i\beta \mathbf{D}_3 \mathbf{p} &= \mathbf{0}, \\ \mathbf{E}_1 \mathbf{u}_1 + \mathbf{E}_2 \mathbf{u}_2 + i\beta \mathbf{E}_3 \mathbf{u}_3 &= \mathbf{0}. \end{aligned}$$

The array structures used in (3.26) are defined as follows:

$$(3.27) \quad \begin{aligned} (\mathbf{A})_{I,J} &= \langle b_I^V, W_m b_J^V \rangle_\omega, & (\mathbf{K})_{I,J} &= \langle b_I^V, \tilde{\Delta} b_J^V \rangle_\omega, \\ \mathbf{C} &= i\beta \mathbf{A} - \frac{1}{\text{Re}} (\mathbf{K} - \beta^2 \mathbf{I}), \\ (\mathbf{D}_1)_{I,J} &= \frac{1}{L} \langle b_I^V, [\partial_\xi - a(\eta) g_1(\xi) \partial_\eta] b_J^P \rangle_\omega, \\ (\mathbf{D}_2)_{I,J} &= \frac{1}{L} \gamma \langle b_I^V, g_2(\xi) \partial_\eta b_J^P \rangle_\omega, \\ (\mathbf{D}_3)_{I,J} &= \langle b_I^V, b_J^P \rangle_\omega, \end{aligned}$$

$$\begin{aligned}
 (\mathbf{B}_1)_{I,J} &= \frac{1}{L} \langle b_I^V, b_J^V [\partial_\xi - a(\eta)g_1(\xi)\partial_\eta] W_m \rangle_\omega, \\
 (\mathbf{B}_2)_{I,J} &= \frac{1}{L} \gamma \langle b_I^V, b_J^V g_2(\xi)\partial_\eta W_m \rangle_\omega, \\
 (\mathbf{E}_1)_{I,J} &= \frac{1}{L} \langle b_I^P, [\partial_\xi - a(\eta)g_1(\xi)\partial_\eta] b_J^V \rangle_\omega, \\
 (\mathbf{E}_2)_{I,J} &= \frac{1}{L} \gamma \langle b_I^P, g_2(\xi)\partial_\eta b_J^V \rangle_\omega, \\
 (\mathbf{E}_3)_{I,J} &= \langle b_I^P, b_J^V \rangle_\omega.
 \end{aligned}
 \tag{3.37}$$

[cont.]

Note that for all arrays defined by the formulas (3.27) the range of indices is $I, J = 1, \dots, N$.

The algebraic eigenvalue problem (3.26) contains $4N$ equations. On the basis of the main flow calculations, a reasonable accuracy should be achieved with the value of N around 3000–4000, thus the total dimension of the eigenvalue problem (3.26) is expected to exceed 10^4 . Since the arrays (3.27) are dense, the solution of the problem of this size is quite demanding in both computational resources and the memory storage. Thus, an attempt to reduce the dimension of the problem is worth considering.

We will show that the algebraic eigenvalue problem (3.26) can be replaced by an equivalent problem of the halved size. Here, we mean a size reduction technique which is based on the elimination of the part of the unknowns rather than the usage of possible symmetries (which may or may not exist) of the flow domain.

There are basically two ways to achieve this goal. One method is to follow the procedure proposed by TATSUMI and YOSHIMURA [24] for the rectangular channel flow and transform the original stability equations (2.15) into the system of coupled fourth-order partial differential equations for the amplitude functions \hat{u} and \hat{v} . However, for the transversely corrugated channel, this approach is not convenient for two following reasons. First, the domain transformation would lead to horribly complicated expressions of the 4th-order differential operators. Secondly, the transformed boundary conditions at the wavy walls will couple in a complicated way both components of the velocity. It means that the analytical construction of the velocity basic functions satisfying identically homogeneous boundary conditions would be not possible.

An alternative approach is to transform algebraically the problem (3.26) into an equivalent smaller problem. In the first step, the pressure unknowns (the vector \mathbf{p}) are eliminated. To this aim, we multiply the first block equation in the system (3.26) by the matrix \mathbf{E}_1 , the second one by the matrix \mathbf{E}_2 , the third one by the matrix $i\beta\mathbf{E}_3$ and then add all three block equations together. This operation is exactly the discrete counterpart of applying the divergence operator to

the linearized Navier–Stokes Equation. As a result, one obtains the linear system

$$(3.28) \quad \mathbf{S}\mathbf{p} = -(\mathbf{E}_1\mathbf{C} + i\beta\mathbf{E}_3\mathbf{B}_1)\mathbf{u}_1 - (\mathbf{E}_2\mathbf{C} + i\beta\mathbf{E}_3\mathbf{B}_2)\mathbf{u}_2 - i\beta\mathbf{E}_3\mathbf{C}\mathbf{u}_3,$$

where the matrix \mathbf{S} is the algebraic analog of the Laplace operator and is defined as follows:

$$(3.29) \quad \mathbf{S} = \mathbf{E}_1\mathbf{D}_1 + \mathbf{E}_2\mathbf{D}_2 - \beta^2\mathbf{E}_3\mathbf{D}_3,$$

Note that all terms with the complex frequency σ have disappeared because the vectors \mathbf{u}_1 , \mathbf{u}_2 and \mathbf{u}_3 satisfy the last block equation of the system (3.26), which is the algebraic counterpart of the continuity equation.

The matrix \mathbf{S} is nonsingular, hence the vector \mathbf{p} can be determined from (3.28) as

$$(3.30) \quad \mathbf{p} = \mathbf{H}_1\mathbf{u}_1 + \mathbf{H}_2\mathbf{u}_2 + \mathbf{H}_3\mathbf{u}_3,$$

where

$$(3.31) \quad \begin{aligned} \mathbf{H}_1 &= -\mathbf{S}^{-1}(\mathbf{E}_1\mathbf{C} + i\beta\mathbf{E}_3\mathbf{B}_1), \\ \mathbf{H}_2 &= -\mathbf{S}^{-1}(\mathbf{E}_2\mathbf{C} + i\beta\mathbf{E}_3\mathbf{B}_2), \\ \mathbf{H}_3 &= -i\beta\mathbf{S}^{-1}\mathbf{E}_3\mathbf{C}. \end{aligned}$$

This way, the eigenvalue problem (3.26) has been replaced by the smaller problem (the size is $3N$) of the following block structure:

$$(3.32) \quad \begin{bmatrix} \mathbf{C} + \mathbf{D}_1\mathbf{H}_1 & \mathbf{D}_1\mathbf{H}_2 & \mathbf{D}_1\mathbf{H}_3 \\ \mathbf{D}_2\mathbf{H}_1 & \mathbf{C} + \mathbf{D}_2\mathbf{H}_2 & \mathbf{D}_2\mathbf{H}_3 \\ \mathbf{B}_1 + i\beta\mathbf{D}_3\mathbf{H}_1 & \mathbf{B}_2 + i\beta\mathbf{D}_3\mathbf{H}_2 & \mathbf{C} + i\beta\mathbf{D}_3\mathbf{H}_3 \end{bmatrix} \begin{bmatrix} \mathbf{u}_1 \\ \mathbf{u}_2 \\ \mathbf{u}_3 \end{bmatrix} = i\sigma \begin{bmatrix} \mathbf{u}_1 \\ \mathbf{u}_2 \\ \mathbf{u}_3 \end{bmatrix}.$$

Although the size of the eigenvalue problem has been reduced, the form (3.32) is still not suitable for practical calculations. To understand why the size reduction procedure should be continued, observe that the following matrix equality holds:

$$(3.33) \quad [\mathbf{E}_1 \ \mathbf{E}_2 \ i\beta\mathbf{E}_3] \begin{bmatrix} \mathbf{C} + \mathbf{D}_1\mathbf{H}_1 & \mathbf{D}_1\mathbf{H}_2 & \mathbf{D}_1\mathbf{H}_3 \\ \mathbf{D}_2\mathbf{H}_1 & \mathbf{C} + \mathbf{D}_2\mathbf{H}_2 & \mathbf{D}_2\mathbf{H}_3 \\ \mathbf{B}_1 + i\beta\mathbf{D}_3\mathbf{H}_1 & \mathbf{B}_2 + i\beta\mathbf{D}_3\mathbf{H}_2 & \mathbf{C} + i\beta\mathbf{D}_3\mathbf{H}_3 \end{bmatrix} = [\mathbf{0} \ \mathbf{0} \ \mathbf{0}].$$

In the above, the left factor is the rectangular matrix (having N rows and $3N$ columns), while the results of the matrix multiplication is the rectangular zero matrix. To verify (3.33), let us follow the calculations for the first block column

$$(3.34) \quad \begin{aligned} & \mathbf{E}_1(\mathbf{C} + \mathbf{D}_1\mathbf{H}_1) + \mathbf{E}_2\mathbf{D}_2\mathbf{H}_1 + i\beta\mathbf{E}_3(\mathbf{B}_1 + i\beta\mathbf{D}_3\mathbf{H}_1) \\ &= \mathbf{E}_1\mathbf{C} - \mathbf{E}_1\mathbf{D}_1\mathbf{S}^{-1}(\mathbf{E}_1\mathbf{C} + i\beta\mathbf{E}_3\mathbf{B}_1) - \mathbf{E}_2\mathbf{D}_2\mathbf{S}^{-1}(\mathbf{E}_1\mathbf{C} + i\beta\mathbf{E}_3\mathbf{B}_1) \\ & \quad + i\beta\mathbf{E}_3\mathbf{B}_1 + \beta^2\mathbf{E}_3\mathbf{D}_3\mathbf{S}^{-1}(\mathbf{E}_1\mathbf{C} + i\beta\mathbf{E}_3\mathbf{B}_1) \\ &= \mathbf{E}_1\mathbf{C} + i\beta\mathbf{E}_3\mathbf{B}_1 - \underbrace{(\mathbf{E}_1\mathbf{D}_1 + \mathbf{E}_2\mathbf{D}_2 - \beta^2\mathbf{E}_3\mathbf{D}_3)}_{\mathbf{S}}\mathbf{S}^{-1}(\mathbf{E}_1\mathbf{C} + i\beta\mathbf{E}_3\mathbf{B}_1) = \mathbf{0}. \end{aligned}$$

We conclude that each row of the left rectangular matrix in the (3.33) is the left eigenvector associated to the nonphysical zero eigenvalue of the problem (3.32). Since the rank of the rectangular matrix is N , the multiplicity of the zero eigenvalue is also equal to N . In other words, the eigenvalue problem (3.32) has dimension equal to $3N$ but it contains the information only about (at most) $2N$ normal modes.

The remedy is to eliminate one of the velocity components. More specifically, the last block of the equations in (3.26) can be used to express the vector \mathbf{u}_3 by the vectors \mathbf{u}_1 and \mathbf{u}_2 :

$$(3.35) \quad \mathbf{u}_3 = \frac{i}{\beta} \mathbf{E}_3^{-1} (\mathbf{E}_1 \mathbf{u}_1 + \mathbf{E}_2 \mathbf{u}_2).$$

After elimination of \mathbf{u}_3 from the system (3.32), we arrive at the following final form of the eigenvalue problem:

$$(3.36) \quad \begin{bmatrix} \mathbf{C} + \mathbf{D}_1 \left(\mathbf{H}_1 + \frac{i}{\beta} \mathbf{H}_3 \mathbf{E}_3^{-1} \mathbf{E}_1 \right) & \mathbf{D}_1 \left(\mathbf{H}_2 + \frac{i}{\beta} \mathbf{H}_3 \mathbf{E}_3^{-1} \mathbf{E}_2 \right) \\ \mathbf{D}_2 \left(\mathbf{H}_1 + \frac{i}{\beta} \mathbf{H}_3 \mathbf{E}_3^{-1} \mathbf{E}_1 \right) & \mathbf{C} + \mathbf{D}_2 \left(\mathbf{H}_2 + \frac{i}{\beta} \mathbf{H}_3 \mathbf{E}_3^{-1} \mathbf{E}_2 \right) \end{bmatrix} \begin{bmatrix} \mathbf{u}_1 \\ \mathbf{u}_2 \end{bmatrix} = i\sigma \begin{bmatrix} \mathbf{u}_1 \\ \mathbf{u}_2 \end{bmatrix}.$$

The size of the problem (3.36) is $2N$, i.e., the original size of (3.26) has been halved as promised. By finding the eigensolutions of (3.36), one obtains the complex frequencies of the normal modes as well as x and y components of the associated velocity disturbances. For each particular normal mode, the z component of the velocity disturbance field can be determined using the formula (3.35) and the pressure field can be found from (3.30).

The size reduction described above is of a great practical value only if we intend to determine the whole spectrum or – at least – its sufficiently numerous subset. In such circumstances, the application of the QZ iterative algorithm seems justified. The highly optimized implementations of this algorithm have been available for years in various numerical libraries, e.g., in the LAPACK library. Since the problem (3.36) is complex and nonsymmetric, reduction of its size by the factor of two will result in significant decrease of the computational time (more than one order of magnitude). A substantial savings in terms of memory will be also achieved, even though a few additional matrices of the dimension N need to be constructed and stored.

On the other hand, the calculations of the full spectrum are definitely not a reasonable way to assess the parametric variation of just one or even a few selected normal modes. Indeed, such computations would necessitate a repetitive re-assembling of the block matrix in (3.36), which in turn requires the re-construction of the matrices \mathbf{H}_1 , \mathbf{H}_2 and \mathbf{H}_3 . Note, however, that single re-

construction process consists in solving $O(N)$ linear system (with the matrix \mathbf{S}) of the dimension equal N , so the numerical cost scales with N at like $O(N^3)$.

Much more efficient way to determine a single normal mode is to use the Inverse Power Method (IPM). The parametric variation of an invariant subspace spanned by a few selected eigenmodes can be efficiently followed by means of the IPM's generalization known as the Method of Subspace Iterations [26]. In the current study, only the first method is used, i.e., normal modes of interest have been traced separately through the parameter space. In the IPM, each normal mode is evaluated by an iterative procedure initialized from the solution corresponding to a previous value of a parameter. For the sake of convenient reference, such procedure, designed for the complex eigenvalue problem $\mathbf{M}\mathbf{x} = \lambda\mathbf{x}$, can be summarized as follows.

Having the approximate eigenvalue $\tilde{\lambda}$, set the normalized vector x^0 , the complex number $\delta^0 = 0$, and perform the following computations ($k = 0, 1, \dots$):

1. Solve the linear system $(\mathbf{M} - \tilde{\lambda}\mathbf{I})\mathbf{z}^{k+1} = \mathbf{x}^k$.
2. Find the normalization factor δ^{k+1} , i.e., such (usually complex) number that the vector $\mathbf{x}^{k+1} = \mathbf{z}^{k+1}/\delta^{k+1}$ is normalized.
3. Check convergence: if $|\delta^{k+1} - \delta^k|/|\tilde{\lambda}| \leq \varepsilon$ then calculate the eigenvalue $\lambda = \tilde{\lambda} + \delta^{k+1}$ and \mathbf{x}^{k+1} is the associated (and normalized) eigenvector; otherwise go back to the step 1.

Note that the particular form of the normalization used in the IPM is not important, except when it should uniquely fix both the magnitude and the phase of a complex vector \mathbf{x}^{k+1} .

The Inverse Power Method can be applied directly to the reduced system (3.36), but in view of the above mentioned cost of the re-generation of the block matrix in (3.36), it is actually much more efficient to apply the IPM directly to the original system (3.26). The key ingredient of the computational procedure is the efficient solver of the relevant linear system (step 1 of the IPM). To this aim, assume that $(\sigma_0; \mathbf{u}_1, \mathbf{u}_2, \mathbf{u}_3, \mathbf{p})$ is the available approximation of a selected normal mode. Then the linear system solved in each iteration step of the IPM is

$$(3.37) \quad \begin{aligned} \mathbf{C}_\sigma \mathbf{w}_1 + \mathbf{D}_1 \mathbf{q} &= \mathbf{u}_1, \\ \mathbf{C}_\sigma \mathbf{w}_2 + \mathbf{D}_2 \mathbf{q} &= \mathbf{u}_2, \\ \mathbf{C}_\sigma \mathbf{w}_3 + \mathbf{B}_1 \mathbf{w}_1 + \mathbf{B}_2 \mathbf{w}_2 + i\beta \mathbf{D}_3 \mathbf{q} &= \mathbf{u}_3, \\ \mathbf{E}_1 \mathbf{w}_1 + \mathbf{E}_2 \mathbf{w}_2 + i\beta \mathbf{E}_3 \mathbf{w}_3 &= \mathbf{0}, \end{aligned}$$

where $\mathbf{C}_\sigma = i\beta\mathbf{A} - \frac{1}{\text{Re}}(\mathbf{K} - \beta^2\mathbf{I}) - i\sigma_0\mathbf{I}$. The exact solution of (3.37) can be found in three steps as follows:

- 1) solve the linear systems

$$\mathbf{C}_\sigma \hat{\mathbf{w}}_1 = \mathbf{u}_1, \quad \mathbf{C}_\sigma \hat{\mathbf{w}}_2 = \mathbf{u}_2, \quad \mathbf{C}_\sigma \hat{\mathbf{w}}_3 = \mathbf{u}_3;$$

2) solve the linear system

$$\mathbf{S} \mathbf{q} = \mathbf{E}_1 \hat{\mathbf{w}}_1 + \mathbf{E}_2 \hat{\mathbf{w}}_2 + i\beta \mathbf{E}_3 \hat{\mathbf{w}}_3,$$

where

$$\mathbf{S} = \mathbf{E}_1 \mathbf{H}_1 + \mathbf{E}_2 \mathbf{H}_2 + \mathbf{E}_3 \mathbf{H}_3$$

and

$$\mathbf{H}_1 = \mathbf{C}_\sigma^{-1} \mathbf{D}_1, \quad \mathbf{H}_2 = \mathbf{C}_\sigma^{-1} \mathbf{D}_2, \quad \mathbf{H}_3 = -\beta \mathbf{C}_\sigma^{-1} [\beta \mathbf{D}_3 + i(\mathbf{B}_1 \mathbf{H}_1 + \mathbf{B}_2 \mathbf{H}_2)];$$

3) solve the linear systems

$$\mathbf{C}_\sigma \mathbf{w}_1 = \mathbf{u}_1 - \mathbf{D}_1 \mathbf{q}, \quad \mathbf{C}_\sigma \mathbf{w}_2 = \mathbf{u}_2 - \mathbf{D}_2 \mathbf{q},$$

$$\mathbf{C}_\sigma \mathbf{w}_3 = \mathbf{u}_3 - \mathbf{B}_1 \mathbf{w}_1 - \mathbf{B}_2 \mathbf{w}_2 - i\beta \mathbf{D}_3 \mathbf{q}.$$

The convergence tests have been performed in order to find the values of the discretization parameters N_ξ and N_η , giving a reasonable accuracy of evaluation of the complex frequency corresponding to the most amplified normal mode. The tests have been conducted for both symmetric and one-sided wall waviness. The geometry of the corrugation chosen for the tests renders the flow particularly unstable at this Reynolds number (see the analysis in the next section). The computed values of the complex frequency of the most amplified normal mode are presented in the Table 1.

Table 1. Results of the convergence tests.

Symmetric wall corrugation: $L = 20$, $M = 9$, $S = 0.4$. Streamwise wave number $\beta = 0.6$			
	$N_\eta = 25$	$N_\eta = 29$	$N_\eta = 35$
$N_\xi = 99$	$0.49292110 + 0.01728863i$	$0.49292110 + 0.01728863i$	$0.42292110 + 0.01728863i$
$N_\xi = 109$	$0.49327893 + 0.01706665i$	$0.49327892 + 0.01706666i$	$0.49327892 + 0.01706666i$
$N_\xi = 119$	$0.49348171 + 0.01692805i$	$0.49348170 + 0.01692806i$	$0.49348170 + 0.01692806i$
$N_\xi = 129$	$0.49347311 + 0.01693104i$	$0.49347310 + 0.01693105i$	
One-sided wall corrugation: $L = 20$, $M = 8$, $S = 0.8$. Streamwise wave number $\beta = 0.5$			
$N_\xi = 99$	$0.38166243 + 0.00940009i$	$0.38166242 + 0.00940008i$	$0.38166242 + 0.00940008i$
$N_\xi = 109$	$0.38179347 + 0.00933710i$	$0.38179345 + 0.00933710i$	$0.38179345 + 0.00933710i$
$N_\xi = 119$	$0.38173289 + 0.00932563i$	$0.38173287 + 0.00932560i$	$0.38173286 + 0.00932559i$
$N_\xi = 129$	$0.38170551 + 0.00932725i$	$0.38170548 + 0.00932723i$	$0.38170547 + 0.00932723i$

It can be seen that the convergence with respect to the number N_η is achieved easily, while the convergence with respect to the number N_ξ is more demanding.

Such “anisotropic” behavior is actually expected since, for the large aspect ratios of the channel section, numerous higher-order polynomials are necessary to capture all the flow details in the spanwise direction. Setting of $N_\xi = 119$ and $N_\eta = 29$ has been eventually chosen, which seems to be a reasonable compromise between accuracy and computational efficiency. With such setting, the number of correct significant digits in the evaluation of the complex frequency is never worse than three. This is not much, yet we believe that it is sufficient to justify our final conclusions. It should be also noted that all calculations presented in this work have been obtained by the numerical code which has been designed for a general geometry and thus ignores intrinsic symmetries possessed by the flow cases considered. The convergence of the eigenvalue evaluation could be certainly improved by the method designed specially for flows with such symmetries.

4. Discussion of the obtained results

4.1. Forms of the wall corrugation

In this section, we discuss the results of the computations of the main flow and its linear stability analysis. The discussion concerns two kinds of the transversely oriented wall corrugation defined in the Sec. 2.2. More specifically, the wall corrugation has sinusoidal shape and can be applied symmetrically to both the bottom and top walls

$$(4.1) \quad y_t(x) \equiv h(x) = 1 + S \cos(M\pi x/L) = -y_b(x),$$

or just to the top wall, while the bottom wall remains flat

$$(4.2) \quad y_t(x) \equiv h(x) = 2 + S \cos(M\pi x/L), \quad y_b(x) \equiv 0.$$

The value of the corrugation amplitude S is assumed to be positive for odd values of M and negative for even values of M . It means that the height of the sidewalls is the smallest possible, i.e., it is equal to $2 - 2|S|$ for the symmetric waviness and or it is equal to $2 - |S|$ for the one-sided waviness.

4.2. Properties of the main flow

The most characteristic feature of the flow through the channel with the bottom and top walls corrugated according to the formulae (4.1) or (4.2) is the strong spanwise modulation of the velocity field. For the symmetric corrugation (4.1), this effect is illustrated in Fig. 5, where the velocity profile across the channel is shown. Different solid lines correspond to a different number M of the corrugation periods across the bottom and top walls. The aspect ratio of the channel is equal to $L = 10$ and the corrugation amplitude $S = 0.4$. The reference

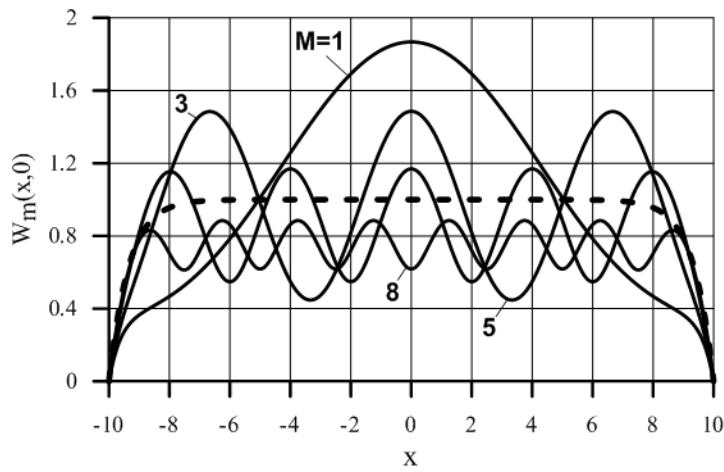


Fig. 5. Main flow velocity distribution across the channel with symmetrically corrugated walls, computed in the symmetry plane $y = 0$. Each line corresponds to a different number M of the corrugation periods. The velocity profile of the flow in the reference rectangular channel is depicted by the thick dashed line (indicated by the symbol R). The geometric parameters are $L = 10$ and $S = 0.4$.

velocity profile of the flow through the rectangular channel is presented by the dashed line.

The velocity field of the main flow in the symmetrically corrugated channel with $L = 10$, $M = 5$ and $S = 0.4$ has been shown also by the contour map in Fig. 6a. The flow through the channel with the same value of the aspect ratio

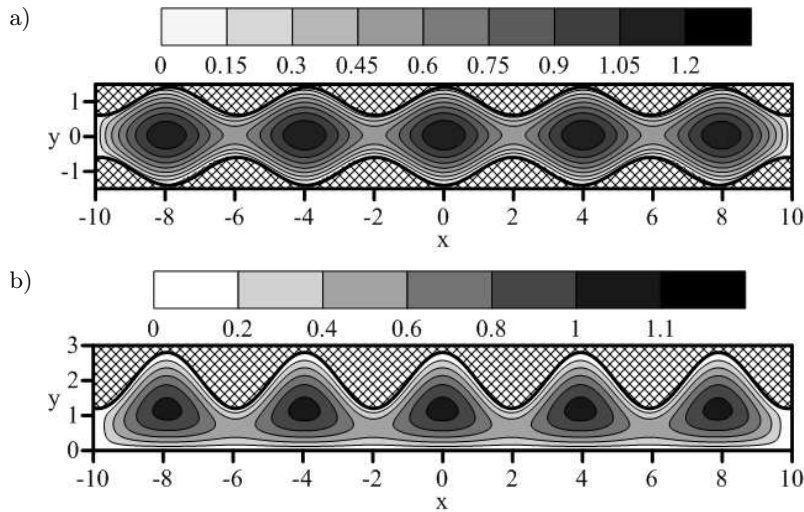


Fig. 6. Contour maps of the main flow velocity magnitude computed for the channel with the aspect ratio $L = 10$ and: a) symmetric corrugation with $M = 5$ and $S = 0.4$, b) one-sided corrugation with $M = 5$ and $S = 0.8$.

L and the number of the corrugation periods M , but with the one-sided wall corrugation (4.2) with the amplitude $S = 0.8$, is shown in Fig. 6b. Strong modulation of the flow velocity in the transversal direction, as well as the presence of inflection points is evident from all these plots. It can be also observed for short-wave corrugations, i.e., corresponding to larger values of M (like $M = 8$), that the modulation amplitude and the average value of the flow velocity are visibly smaller. This effect translates directly to the reduction of the flow rate or – equivalently – to the rise of hydraulic resistance. On the other hand, if the wavelength of the wall corrugation rises, then the flow resistance drops and for sufficiently large wavelength (small values of M) it becomes smaller than that for the rectangular channel of the same aspect ratio. This effect is demonstrated in Fig. 7a and 7b, respectively, for the symmetric and one-sided wall corrugation. The aspect ratio of the channel section is $L = 10$. It can be concluded from Fig. 7a that the sinusoidal symmetric wall corrugation (4.1) diminishes the flow resistance in such a channel, as long as the number of corrugation periods M is not larger than 4. The gain in the flow rate computed for $M = 1$ and the amplitude $S = 0.5$ is the largest and exceeds by 40% the flow rate in the rectangular channel with the same aspect ratio! On the other hand, using corrugation with shorter periods (M larger than 4) leads to the flow rate reduction, i.e., the flow resistance increases. In particular, for $M = 8$ and the amplitude $S = 0.5$, the flow rate drops under 70% of the flow rate in the rectangular channel. In case of one-sided wall corrugation, the effect is similar,

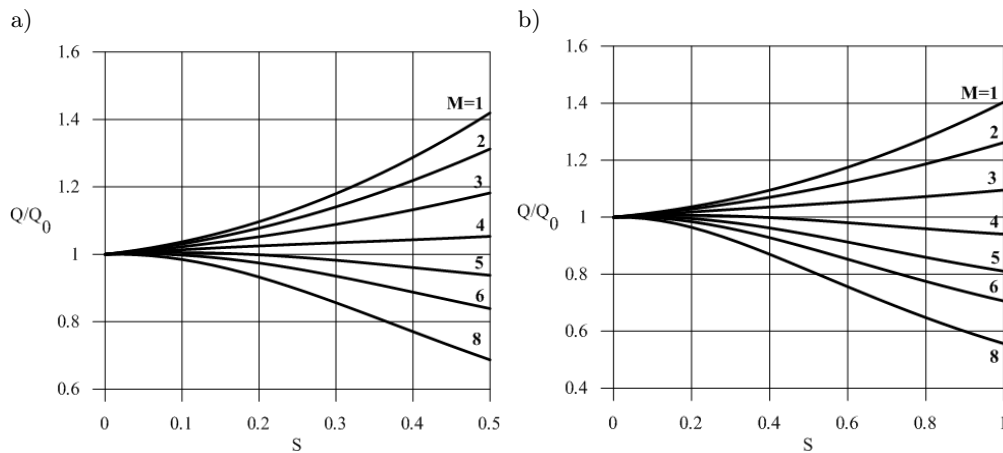


Fig. 7. The effect of transversal wall corrugation on the hydraulic resistance of the main flow. The ratio of the volumetric flow rate to the flow rate of the reference rectangular channel is plotted versus the amplitude S of the corrugation. The aspect ratio of the channel section is $L = 10$. Lines in the plot correspond to a different number M of the corrugation periods. Two cases are shown: a) symmetric corrugation and b) one-sided corrugation.

however, the “neutral” number of the corrugation periods M seems to be shifted a bit into longer wavelengths: the corrugation with $M = 4$ causes now a slight increase rather than reduction of the flow resistance. More details about the impact of the transversely oriented wall corrugation on the hydraulic resistance of the channel flow will be provided in the paper [27]. Also, it should be noted that the relation between the flow resistance and the number of the corrugation periods M (or the corrugation wavelength) is generally consistent with the earlier author’s findings concerning the flow through the spanwise-periodic channel (see [22]).

4.3. Linear stability characteristics

In this section, the results of the linear stability analysis are presented. The investigation is focused mostly on the stability properties of the flow in the channels with large aspect ratios: the considered cases are $L = 10$ and $L = 20$. The stability analysis has been conducted numerically in the following order. First, the normal modes most susceptible for amplification by transversely oriented wall corrugation have been identified. Next, the range of the streamwise wave number β corresponding to the unstable normal mode has been determined for a different number M of the corrugation periods across the channel. The analysis has been concluded with the calculation of the neutral stability curves in the $\text{Re} - \beta$ plane and determination of sample flow patterns.

For sufficiently large aspect ratios, the low-Reynolds-number instability can be expected in roughly the same region of the parameter space as it was found for the flow in the periodic channel. It has been demonstrated in [21] and [22] that the unstable normal mode of the periodic channel flow is related to the particular Squire mode from the Poiseuille spectrum. The wave vector of this mode is $\mathbf{k} = [k_x, k_y, k_z] = [0, 0, \beta]$. The values of the streamwise wavenumber β corresponding to the mode most susceptible for destabilization has been computed to be around 0.4 and the most destabilizing wavelength of the periodic wall corrugation is about 3 times larger than the average channel height.

The stability analysis of the flow in the corrugated channel with sidewalls has confirmed the expected parametric localization of the instability region. In particular, the complex frequencies of the normal modes, which are most susceptible for the low-Re destabilization by wall deformation, have been identified in the analogous part of spectrum of the rectangular channel flow. These frequencies, computed for $L = 20$, $\beta = 0.6$ and $\text{Re} = 100$, are indicated in the plot presented in Fig. 8. It has been found that the attenuation rates of the corresponding normal modes can be extremely sensitive to the wall corrugation

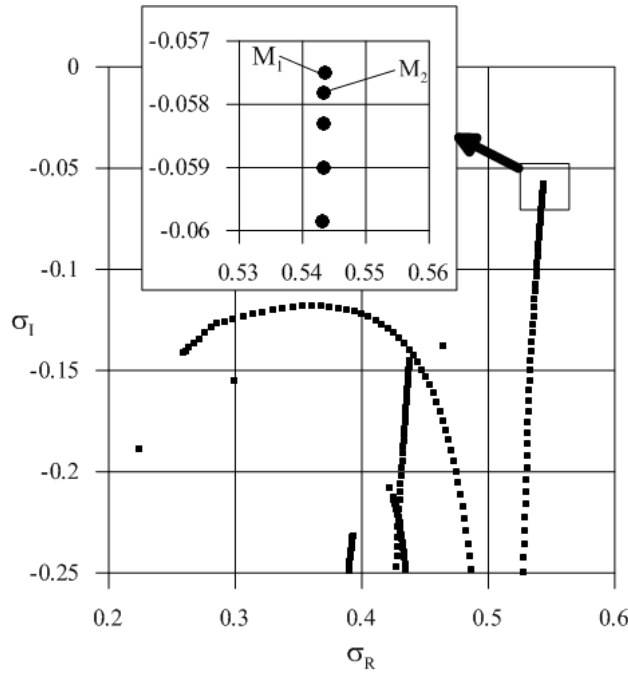


Fig. 8. Eigenvalues (complex frequencies) associated to the normal modes of the flow in the rectangular channel. Only the modes with $\sigma_I \geq -0.25$ are shown. The channel section aspect ratio is $L = 20$, the Reynolds number is $Re = 100$ and the streamwise wave number is $\beta = 0.6$. The eigenvalues corresponding to the normal modes which are the most susceptible to destabilization by transversely oriented wall corrugations are indicated in the zoomed part of the plot.

described by (4.1) or (4.2), especially for appropriately chosen number M of the corrugation periods. Plots in Fig. 9 illustrate this effect for the flow in the channel with the aspect ratio $L = 20$ and the Reynolds number $Re = 100$. The plots in Fig. 9a have been computed for the symmetric wall corrugation with $M = 9$ and the streamwise wave number $\beta = 0.6$. It can be observed that the mode M_1 becomes unstable when the amplitude S exceeds the value of 0.23. For S larger than 0.27 also the mode M_2 is unstable. Both modes remain unstable for the corrugation amplitudes rising up to 0.5, however the largest amplification rate is attained at $S = 0.425$ and then slowly diminishes. Similar features are observed in Fig. 9b where the analogous results obtained for one-sided corrugation with $M = 8$ are presented. This time, the streamwise wave number is $\beta = 0.5$. The mode M_1 loses stability when the amplitude S becomes larger than 0.46, i.e., the amplitude is doubled in comparison with symmetric corrugation. The second mode M_2 becomes unstable when the amplitude S is larger than 0.62. Similarly to the symmetric case, the amplification rate σ_I of both modes attains the maximum at nearly the same value of the corrugation amplitude, i.e., when

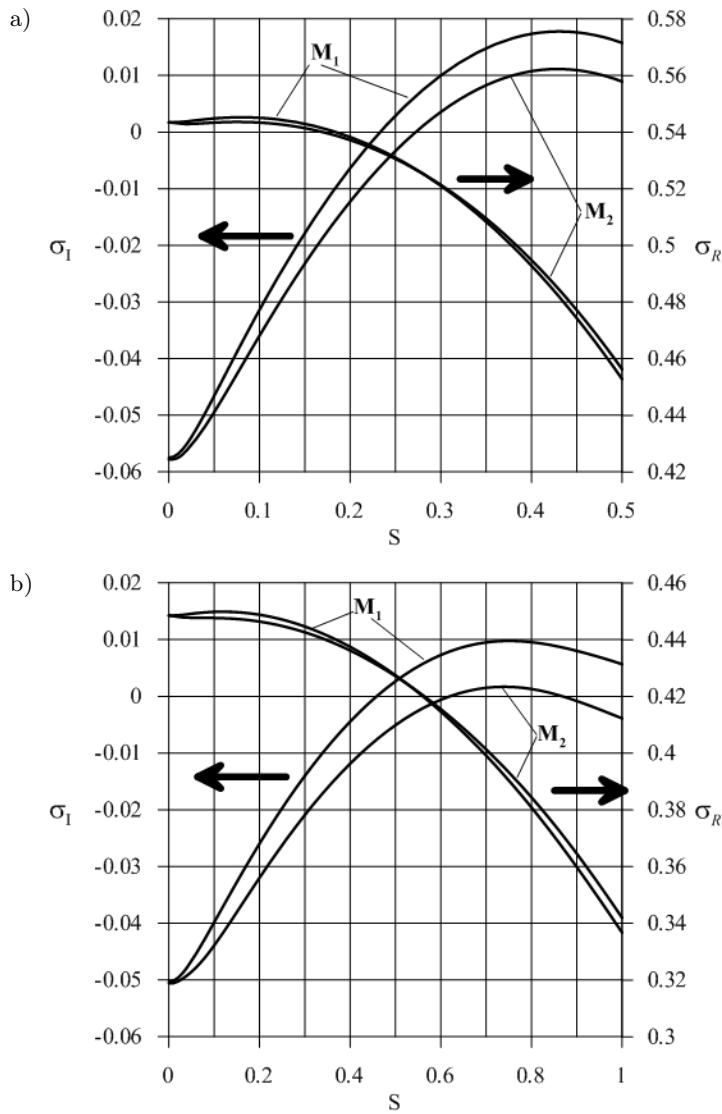


Fig. 9. Complex frequency of two most amplified normal modes plotted versus the amplitude S : a) symmetric corrugation with $M = 9$ wavelengths across the channel, b) one-sided corrugation with $M = 8$ wavelengths across the channel. In both cases, the aspect ratio is $L = 20$ and the Reynolds number is $Re = 100$. The streamwise wave number is: a) $\beta = 0.6$, b) $\beta = 0.5$.

$S = 0.75$. For larger amplitudes, the amplification rate slowly diminishes and for the mode M_2 is becomes negative (i.e., this mode is stable again) when S is larger than 0.86.

In both cases of the wall corrugation, the unstable modes have nonzero real parts of their complex frequencies, i.e., they have the form of travelling

disturbance waves. The phase speed of the disturbance wave (defined by the ratio $v_{ph} = \sigma_R/\beta$) is nearly the same for both modes, irrespectively of the variant of the corrugation. This speed generally diminishes with the corrugation amplitude S (except for the small values of S where the slight increase of σ_R can be noticed). For the rectangular channel ($S = 0$), the phase speed of both modes is close to 0.9, while in the conditions of the maximal corrugation considered, it drops to the value of 0.75 in the symmetric case and 0.68 in the one-sided case. In such conditions the disturbances described by the mode M_2 travel along the channel slightly faster than those corresponding to the mode M_1 .

In the remaining part of this section, the parametric study of the stability characteristics of the most amplified mode M_1 is conducted. The parametric variation of the amplification rate of this mode σ_I with respect to the streamwise wave number β has been presented in Fig. 10. All plots have been obtained for the Reynolds number $Re = 100$. The plot on Fig. 10a has been computed for the channel aspect ratio $L = 10$ and symmetric corrugation with the amplitude $S = 0.4$. It can be seen that the strongest destabilization effect is achieved when $M = 5$. This corresponds to the corrugation period two times larger than the average height of the channel. The most amplified mode has the streamwise wave number $\beta = 0.7$. Other values of M which can destabilize the flow at the Reynolds numbers $Re = 100$ are also shown. The following rule is evident: the corrugation with longer/shorter period (smaller/larger M) destabilizes mostly the mode with longer/shorter wavelength (smaller/larger streamwise wavenumber β). Similar relation has been found earlier for the flow in the spanwise-periodic channel [21, 22].

When the aspect ratio of the channel is increased to $L = 20$, then one obtains the results shown in Fig. 10b. Now, the most destabilizing geometry corresponds to $M = 9$. It means that the wavelength of the optimal corrugation is larger than for $L = 10$. At the same time, the amplification rate assumes larger values. Moreover, the wall corrugations with the number of periods equal to $M = 6$ or $M = 12$ also lead to flow destabilization, while their counterparts for $L = 10$, i.e., $M = 3$ and $M = 6$ do not. This effect is evidently due to the fact that the influence of the sidewalls is reduced with increasing aspect ratio.

In Fig. 10c, analogous results obtained for the one-sided wall corrugation with the amplitude $S = 0.8$ are presented. The strongest destabilization of the mode M_1 is obtained for the corrugation with $M = 8$, i.e., for the corrugation period larger than in the case of symmetric corrugation. Smaller values of the amplification rate are observed as it has been already mentioned. The range on unstable wave numbers β is generally shifted to the left, i.e., one-sided wall corrugation will tend to excite disturbances with larger wavelength.

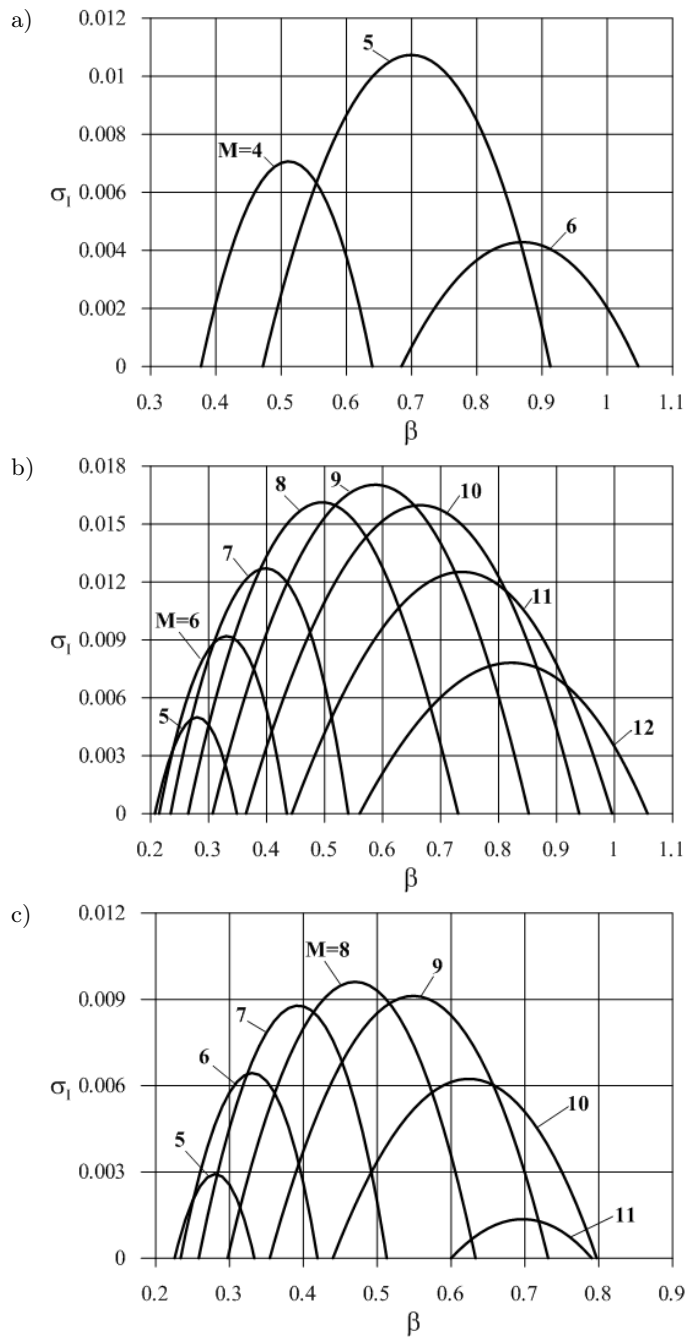


Fig. 10. Amplification rate σ_I of the unstable normal mode plotted versus the streamwise wavenumber β . The Reynolds number is $Re = 100$. Each line corresponds to a different number M of the corrugation periods across the channel. Three cases are shown: a) $L = 10$, symmetric corrugation with $S = 0.4$, b) $L = 20$, symmetric corrugation with $S = 0.4$ and c) $L = 20$, one-sided corrugation with $S = 0.8$.

The results of the linear stability analysis can be conveniently summarized in the form of the neutral stability lines (NSL) in the Re - β plane. Along these lines, the amplification factor of the most amplified mode is zero. In Fig. 11a, the NSL computed for the flow in the channel with the aspect ratio $L = 10$ and the symmetric wall corrugated with $M = 5$ are shown. Each line has been determined for a different value of the corrugation amplitude S . The regions inside the

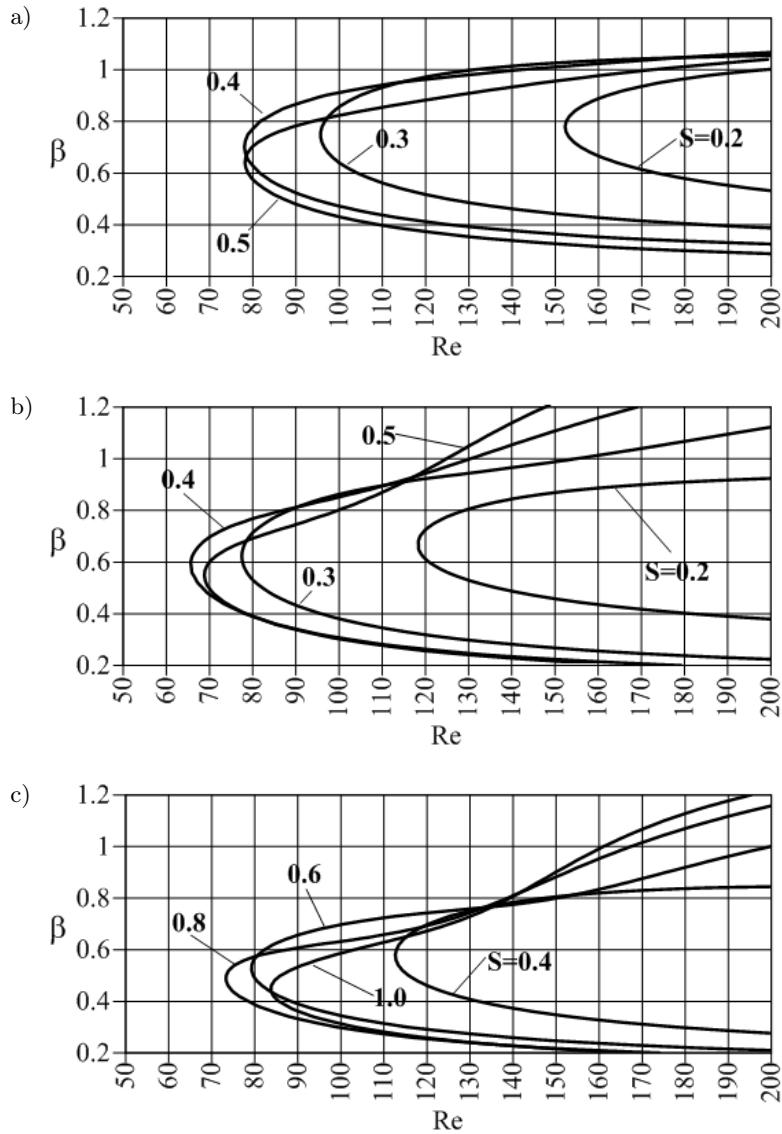


Fig. 11. Neutral stability lines plotted in the plane $Re - \beta$ and computed for different values of the corrugation amplitude S . Three cases are shown: a) $L = 10$ and symmetric corrugation, b) $L = 20$ and symmetric corrugation and c) $L = 20$ and one-sided corrugation.

NSL correspond to linearly unstable flows and the turning point corresponds to the critical conditions. It can be noticed that the minimal value of the critical Reynolds number computed for $S = 0.4$ and $S = 0.5$ is nearly the same and equal about 78.

If the aspect ratio of the channel section is increased to $L = 20$ and the number of corrugation periods is $M = 9$, then the NSL assume the shape shown in Fig. 11b. It can be noticed that the amplitude $S = 0.4$ is the most destabilizing among the considered geometries. The critical Reynolds number drops to 65 which is close to 58 obtained in [22] for the channel of infinite width. The critical value of the streamwise wave number β is close to 0.6.

In Fig. 11c, the neutral stability lines computed for the channel with the aspect ratio $L = 20$ and the one-sided wall corrugation with $M = 8$ are presented. The corrugation amplitudes have been chosen to be doubled amplitudes from Fig. 9b. Comparison with the symmetric case leads to the conclusion that one-sided corrugation is generally less effective in destabilizing the flow. The lowest value of the critical Reynolds number has been obtained for $S = 0.8$ and it is equal about 74. The critical value of the streamwise wave number β is approximately equal 0.48.

Finally, we will discuss shortly the flow disturbance patterns related to the unstable normal modes M_1 and M_2 . We consider only the case of the channel with the aspect ratio $L = 20$ and symmetric wall corrugation. The Reynolds number is $Re = 100$ and the streamwise wave number is $\beta = 0.6$. The velocity field of the disturbances, corresponding to the normal mode M_1 and evaluated in the channel central plane $y = 0$, is shown in Fig. 12. The upper vector plot (a) presents the velocity field of the mode M_1 computed for the flow in the rectangular channel ($S = 0$), while the bottom vector plot (b) shows the velocity pattern of the same mode computed for the corrugated channel with the amplitude $S = 0.4$.

It should be noted that far away from the sidewalls, both patterns of disturbances are very much similar to the disturbance field of the unstable Squire mode in the infinite channel, see [21] and [22]. If there are no sidewalls and no corrugation ($S = 0$), then the only nonzero component of the velocity disturbance field is the x -component, i.e. the component along the spanwise direction. In the presence of the sidewalls, i.e. in the rectangular channel, such form of disturbances is obviously impossible and the flow turns around in the vicinity of the sidewalls, giving rise to a characteristic pattern of a circular motion shown in Fig. 10a. When the wall corrugation is present, then the characteristic array of vortices appears. Again, at the lack of the sidewalls, this pattern is periodic in both the streamwise (z) and spanwise (x) directions. In the channel with sidewalls, the spanwise periodicity is lost and the magnitude of disturbance diminishes while the sidewalls are approached.

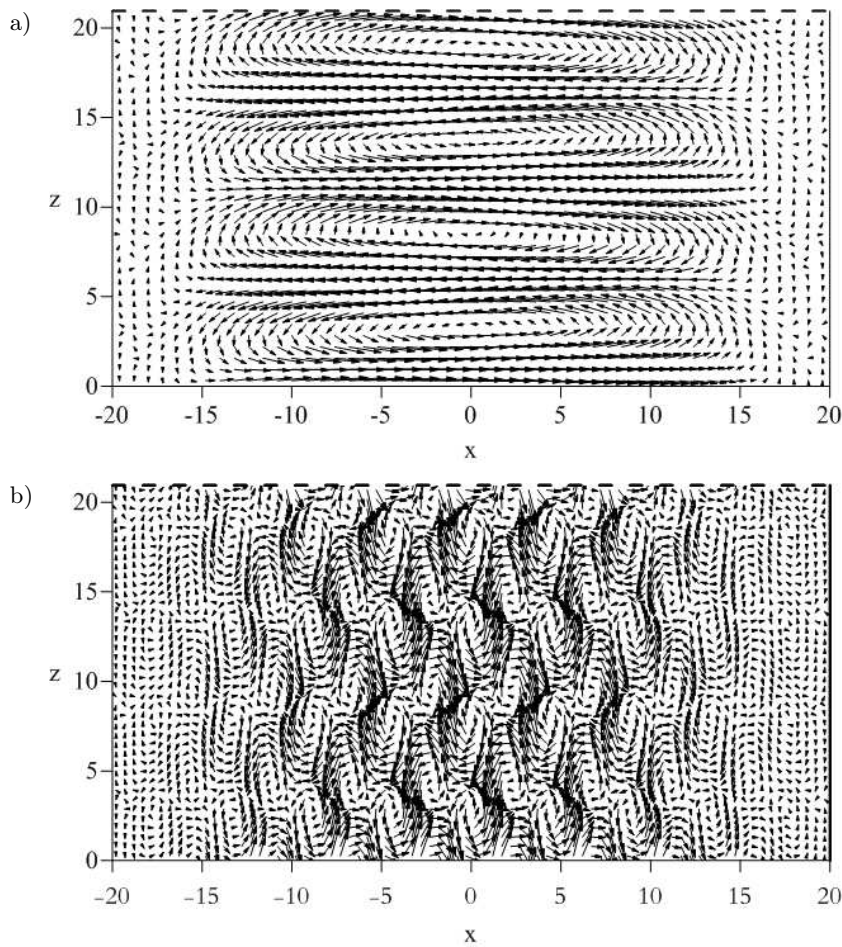


Fig. 12. The velocity field of the most amplified normal mode M_1 evaluated in the plane $y = 0$ for the rectangular (a) and symmetrically corrugated (b) channels. The aspect ratio is $L = 20$ and the corrugation parameters are $M = 9$ and $S = 0.4$. In both cases, the Reynolds number is $Re = 100$ and the streamwise wave number is $\beta = 0.6$.

In Fig. 13, the analogous vortex maps are shown for the second unstable mode M_2 . All parameters are the same as in Fig. 12. In contrast to the mode M_1 , the flow pattern of the mode M_2 does not have any direct counterpart in the flow through the periodic channel. The mode M_2 has an extra symmetry plane $x = 0$, in all other respects the flow pattern in the corrugated channel is similar to the mode M_1 . It should be noted that the normal modes with multiply symmetry planes parallel to the plane $x = 0$ can also exist if the number of the corrugation periods are sufficiently large. These modes are, however, attenuated for the low Reynolds numbers, which are of the main interest in this study.

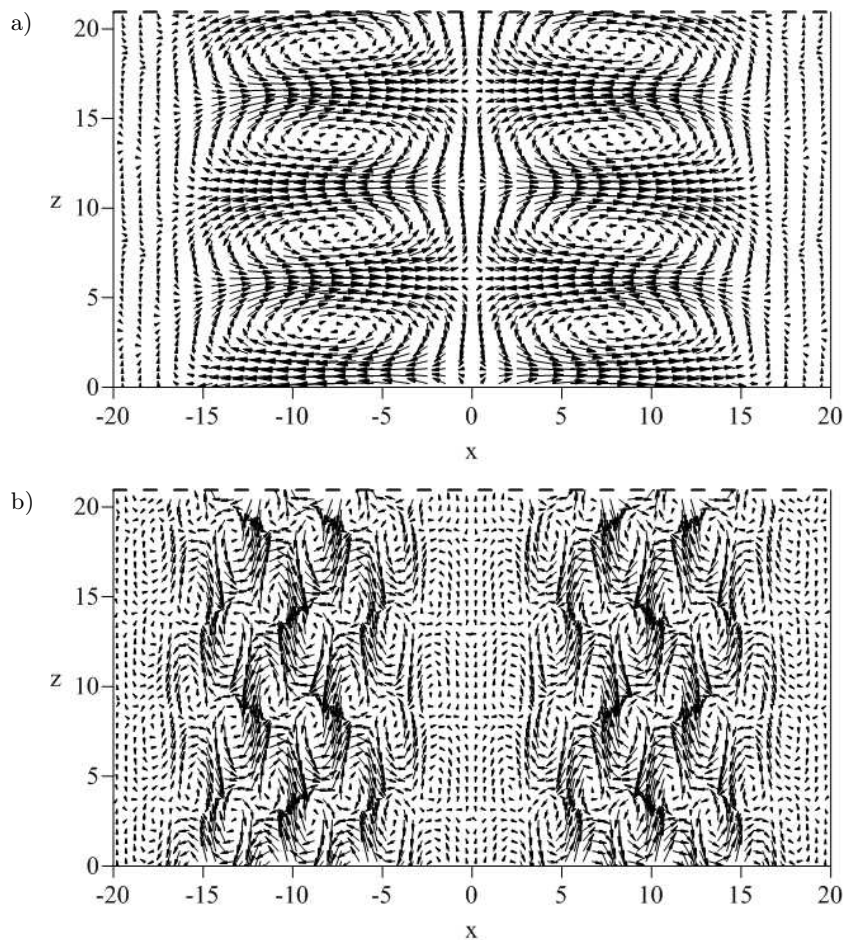


Fig. 13. The velocity field of the second most amplified normal mode M_2 evaluated in the plane $y = 0$ for the rectangular (a) and symmetrically corrugated (b) channels. All settings like in Fig. 12.

5. Summary and conclusions

The instability of the laminar channel flow induced by the transversal wall corrugation, either symmetric or one-sided, has been investigated numerically. In contrast to earlier works, the channel width is assumed to be finite, i.e., the flat sidewalls are present. Both the main flow and the field of flow disturbances are approximated, with spectral accuracy, by means of the Galerkin projection method. The calculations are conducted in the transformed computational domains, where the boundary conditions are satisfied exactly. This approach has allowed for investigation of the wall corrugations with large amplitudes. The unstable normal modes have been identified and their parametric variation has

been determined. The lines of neutral stability (the critical lines) have been computed numerically for selected cases of the wall corrugation. The patterns of disturbance velocity field corresponding to a pair of the most amplified normal modes have been determined.

The main conclusions from this research can be summarized as follows:

- The transversal corrugation of the channel walls can be used to destabilize the flow in the rectangular channel at the Reynolds number lower than 100. The shape of the corrugation which is appropriate for this purpose has only marginal influence on the flow resistance. This property makes the transversal corrugation more attractive than the longitudinal one, where significant increase of the pressure losses is inevitable.
- For sufficiently large aspect ratios, the influence of the sidewalls is weak and the stability properties of the flow do not differ much from the characteristics obtained by SZUMBARSKI in [22] for the flow through periodic channel.
- The most destabilizing form of the corrugation among the configurations studied in this work is the symmetric sinusoidal wall corrugation. When compared to the case of the spanwise-periodic channel, the wavelength of the most destabilizing symmetrical corrugation is smaller and its amplitude is slightly larger. The destabilization effect brought about by the one-sided corrugation, is similar to the effect of symmetric corrugation, providing that the amplitude of the former is twice as large.
- In both variants of the wall corrugation, the maximal effect of flow destabilization (i.e., the largest value of the amplification rate of the most unstable normal mode) is achieved for a certain optimal value of the corrugation amplitude. For the Reynolds number $Re = 100$, the optimal value has been estimated to be about 22% and 38% of the averaged height of the channel for the symmetric and one-sided case, respectively.
- The critical Reynolds number of the flow diminishes with increasing aspect ratio of the channel section approaching asymptotically the value corresponding to the periodic channel. For the aspect ratio $L = 10$, Re_L is equal to 78, but for $L = 20$ it drops to 64 which is close to the asymptotic value of 58 determined by Szumbariski [22]. Since the destabilization effect of one-sided corrugation is weaker, the corresponding value of Re_L is larger, i.e., it is equal 74 for the aspect ratio $L = 20$.
- Similarly to the flow in the periodic channel, the most unstable mode has the form of the streamwise periodic array of the counter-rotating vortex structures. The spanwise periodicity is lost for obvious reasons and the magnitude of the flow disturbance near the sidewalls is small due to the no-slip condition. This pattern of disturbances travels downstream with the phase speed $v_{ph} = \sigma_R/\beta$. For smaller values of the corrugation ampli-

tude S , this velocity is close to 0.9 and it drops with increasing S reaching the value around 0.7 for one-sided corrugation with the amplitude $S = 1.0$. Downstream motion of the vortex structures implies that the flow field developed in the nonlinear saturation process is expected to be fully three-dimensional and oscillatory. Further investigations, including direct numerical simulations, are necessary to find out whether these acquired qualities are sufficient to achieve conditions of effective (chaotic) mixing.

Acknowledgements

This investigation was supported by the Polish Ministry of Science and Education under the project “*Enhancement of the mixing process in micro-flows*”, grant No. N501008733.

References

1. J.L. GOLDSTEIN, E.M. SPARROW, *Heat-mass transfer characteristics for flow in a corrugated wall channel*, Journal of Heat Transfer, **99**, 187–195, 1977.
2. I.J. SOBEY, *On flow through furrowed channels. Part 1: Calculated flow patterns*, Journal of Fluid Mechanics, **96**, 1–26, 1980.
3. K.D. STEPHANOFF, I.J. SOBEY, B.J. BELLHOUSE, *On flow through furrowed channels. Part 2: Observed flow patterns*, Journal of Fluid Mechanics, **96**, 27–32, 1980.
4. T. NISHIMURA, S. MURAKAMI, S. ARAKAWA, Y. KAWAMURA, *Flow observations and mass transfer characteristics in symmetrical wavy-walled channels at moderate Reynolds number for steady flow*, Int. J. Heat and Mass Transfer, **33**, 835–844, 1990.
5. T. NISHIMURA, S. ARAKAWA, S. MURAKAMI, Y. KAWAMURA, *Oscillatory viscous flow in symmetrical wavy-wall channels*, Chemical Engineering Science, **44**, 2211–2224, 1989.
6. T. NISHIMURA, Y. KAWAMURA, *Three-dimensionality of Oscillatory Flow in a Two-dimensional Symmetric Sinusoidal Wavy-Walled Channel*, Exp. Therm. Fluid Sci., **10**, 62–73, 1995.
7. T. NISHIMURA, T. YOSHINO, Y. KAWAMURA, *Numerical flow analysis of pulsatile flow in a channel with symmetric wavy walls at moderate Reynolds numbers*, J. Chem. Eng. Jpn., **20**, 479–485, 1987.
8. T. NISHIMURA, N. KOJIMA, *Mass transfer enhancement in a sinusoidal wavy-walled channel for pulsatile flow*, International Journal of Heat and Mass Transfer, **38**, 1719–1731, 1995.
9. G. WANG, S.P. VANKA, *Convective heat transfer in periodic wavy passages*, International Journal of Heat and Mass Transfer, **38**, 3219–3230, 1995.
10. N. GHADDAR, A. EL-HAJJ, *Numerical Study of Heat Transfer Augmentation of Viscous Flow in Corrugated Channels*, Heat Transfer Engineering, **21**, 35–46, 2000.
11. B. NICENO, E. NOBILE, *Numerical analysis of fluid flow and heat transfer in periodic wavy channel*, International Journal of Heat and Fluid Flow, **22**, 156–167, 2001.
12. K.J. CHO, M. KIM, H.D. SHIN, *Linear stability of two-dimensional steady flow in wavy-walled channel*, Fluid Dynamic Research, **23**, 349–370, 1998.

13. S. BLANCHER, R. CREFF, P. LE QUERE, *Effect of Tollmien-Schlichting wave on convective heat transfer in a wavy channel. Part I: Linear Analysis*, International Journal of Heat and Fluid Flow, **19**, 39–48, 1998.
14. S. BLANCHER, R. CREFF, P. LE QUERE, *Analysis of convective hydrodynamic instabilities in a symmetric wavy channel*, Physics of Fluids, **16**, 3726–3737, 2004.
15. J. SZUMBARSKI, *Immersed boundary approach to stability equations for a spatially periodic viscous flow*, Archives of Mechanics, **54**, 199–222, 2002.
16. A. CABAL, J. SZUMBARSKI, J.M. FLORYAN, *Stability of flow in a wavy channel*, Journal of Fluid Mechanics, **457**, 191–212, 2002.
17. J.M. FLORYAN, *Vortex instability in a diverging-converging channel*, J. Fluid. Mech., **482**, 17–50, 2003.
18. P.R. VISWANATH, *Aircraft viscous drag reduction using riblets*, Progress in Aerospace Sciences, **38**, 571–600, 2002.
19. A.V. BOIKO, G.R. GREK, A.V. DOVGAL, V.V. KOZLOV, *The Origin of Turbulence in Near-Wall Flows*. Springer–Verlag, 2002.
20. U. EHRENSTEIN, *On the linear stability of channel flow over riblets*, Physics of Fluids, **8**, 3194–3196, 1996.
21. J. SZUMBARSKI, *Instability of a viscous liquid flow in a corrugated channel* [in Polish, the habilitation thesis], Published by Warsaw University of Technology, Warszawa, 2007.
22. J. SZUMBARSKI, *Instability of viscous incompressible flow in a channel with transversely corrugated walls*, Journal of Theoretical and Applied Mechanics, **45**, 659–683, 2007.
23. S. BŁOŃSKI, J. SZUMBARSKI, T.A. KOWALEWSKI, *Low-Reynolds-number instability of the laminar flow between wavy walls*, Proceedings of the Sixth International ASME Conference on Nanochannels, Microchannels and Minichannels (ICNMM2008), Darmstadt, Germany, June 23–25, 2008.
24. T. TATSUMI, T. YOSHIMURA, *Stability of the laminar flow in a rectangular duct*, Journal of Fluid Mechanics, **212**, 437–449, 1990.
25. J. SZUMBARSKI, *Stability analysis of a laminar viscous flow in the finite-span wavy channel*, European Fluid Mechanics Conference EFMC-8, Bad Reichenhall, Germany, September 13–16, 2010.
26. Y. SAAD, *Numerical methods for large eigenvalue problems*, Manchester University Press, 1992.
27. J. SZUMBARSKI, S. BŁOŃSKI, T.A. KOWALEWSKI, *On the impact of transversely-oriented wall corrugation on hydraulic resistance of a laminar channel flow*, to be submitted to Archives of Mechanical Engineering, 2011.

Received December 1, 2010; revised version June 23, 2011.
